

A continuous-time solver for quantum impurity models

Philipp Werner, Armin Comanac, Luca De Medici, and Andrew J. Millis
Columbia University, 538 West, 120th Street, New York, NY 10025, USA

Matthias Troyer
Institut für theoretische Physik, ETH Hönggerberg, CH-8093 Zürich, Switzerland
(Dated: January 25, 2020)

We present a new continuous time solver for the quantum impurity models relevant to dynamical mean field theory. The method is based on a stochastic sampling of a perturbation expansion in the impurity-bath hybridization parameter. For the one-orbital Hubbard model, no sign problem is found. Comparisons to Hirsch-Fye quantum Monte Carlo as well as exact diagonalization calculations confirm the accuracy of the new approach and show that it allows an efficient calculation of the Green function even at very low temperatures. Extensions to more general models are discussed.

Numerical computation of dynamical properties of strongly correlated fermion systems is one of the fundamental challenges in condensed matter physics. The exponential growth of the Hilbert space renders exact diagonalizations impossible except for very small systems [1]. When applied directly to lattice models, auxiliary field Monte Carlo methods encounter severe difficulties with the fermionic sign problem [2]. The density matrix reormalization group [3] is powerful for extracting ground state properties of one dimensional systems, but extensions to higher dimensions and dynamics have proven difficult. Over the last decade, a promising new “dynamical mean field” (DMFT) approach has been developed [4, 5, 6]. As shown by Georges, Kotliar and co-workers [6, 7], if the momentum dependence of the self-energy is neglected, $\Sigma(p, \omega) \rightarrow \Sigma(\omega)$, then the solution of the lattice model may be obtained from the solution of a quantum impurity model plus a self-consistency condition.

The dynamical mean field idea led to an explosion of activity [7, 8] because the quantum impurity model is amenable to numerical study. In the DMFT method, the quantum impurity model may be specified by a partition function $Z = \text{Tr} T_\tau e^{-S}$ with action $S = S_F + S_{\text{loc}}$, where

$$S_F = - \int_0^\beta d\tau d\tau' \psi(\tau) F(\tau - \tau') \psi^\dagger(\tau'), \quad (1)$$

$$S_{\text{loc}} = - \int_0^\beta d\tau (\mu \psi^\dagger \psi - U^{abcd} \psi_a^\dagger \psi_b^\dagger \psi_c \psi_d). \quad (2)$$

Note that we have chosen the creation operator basis rather than the more conventional coherent state basis and an unconventional operator ordering in Eq. (1). Our F is related to the usual mean field function G_0^{-1} by $G_0^{-1}(i\omega) = i\omega + \mu - F(-i\omega)$.

The computationally intensive part of the DMFT procedure is the evaluation of the impurity model Green function $G = -\langle T_\tau \psi \psi^\dagger \rangle$. Over the last 15 years, two methods have mainly been used. One is the Hirsch-Fye method [9], in which a (discrete) Hubbard-Stratonovich transformation is used to decouple the four-fermion term of the interaction part. It is then possible to integrate out

the fermion fields, leading to determinants which give the weights associated with the configurations of the auxiliary fields, which are then sampled by a Monte Carlo procedure. While conceptually simple and robust, the method suffers from certain drawbacks. It requires a time discretization, in which the imaginary time interval $[0, \beta]$ is divided into N equally spaced intervals. At low temperatures and strong correlations, the Green functions have a highly non-uniform time dependence, dropping very steeply near the edge points $\tau = 0, \beta$, and varying more slowly in between. The rapid drop means that a very large number of time slices is required, and hence the evaluation of determinants of very large matrices, which is computationally prohibitive. This limits the utility of the algorithm in physically interesting limits. Furthermore, useful decouplings of the general interactions of multiorbital models are lacking. Another approach is an exact diagonalization method [10, 11] in which the continuum of energies in the impurity model is replaced by a discrete set of levels. This method suffers from systematic errors associated with the discrete level spacing, and becomes impractical in the multiorbital case because of the rapid growth of the Hilbert space.

In this paper we explore a continuous-time approach to the solution of the quantum impurity model. The key idea, introduced in the context of bosonic field theories by Prokof'ev *et al.* [12] is to define a formal perturbation expansion for the partition function Z . The terms in this series are then sampled by a Monte Carlo procedure. Rubtsov and co-workers [13] have applied this method to the impurity problems of dynamical mean field theory, expanding in the interaction term. Their algorithm samples fermionic determinants and seems to overcome some of the difficulties mentioned above.

We investigate here the alternative, somewhat less conventional route of treating S_{loc} exactly and expanding in S_F . This expansion generates a series in which a term of order k involves an expectation value, taken with respect to S_{loc} , of k ψ^\dagger operators at times $\tau_{i=1, \dots, k}^s$ and k ψ operators at times $\tau_{i=1, \dots, k}^e$, multiplied by a determinant of a matrix, whose entries are given by F evaluated

at all possible time differences $\tau_m^e - \tau_n^s$. The series can be sampled by a Monte Carlo procedure which inserts or removes $\psi(\tau)F(\tau - \tau')\psi^\dagger(\tau')$ at randomly chosen times.

We illustrate the procedure first for noninteracting spinless fermions, and then proceed to the Hubbard model. Because the spinless fermion model is diagonal in the occupation number basis, we have for $Z^F \equiv Z(\mu = 0, U = 0, \sigma)$

$$Z^F = 2 + \sum_{k=1}^{\infty} \int_0^\beta d\tau_1^s \int_{\tau_1^s}^{\circ\tau_1^s} d\tau_1^e \int_{\tau_1^e}^{\circ\tau_2^s} d\tau_2^s \int_{\tau_2^s}^{\circ\tau_2^e} d\tau_2^e \dots \dots \int_{\tau_{k-1}^e}^{\circ\tau_1^s} d\tau_k^s \int_{\tau_k^s}^{\circ\tau_1^s} d\tau_k^e Z_k^F(\tau_1^s, \tau_1^e; \tau_2^s, \tau_2^e; \dots; \tau_k^s, \tau_k^e), \quad (3)$$

with $Z_k^F(\tau_1^s, \tau_1^e; \tau_2^s, \tau_2^e; \dots; \tau_k^s, \tau_k^e)$ denoting the collection of $k!$ diagrams containing k segments of occupied fermion states, with starting point τ_i^s and end point τ_i^e , $i = 1, \dots, k$. We view the interval $[0, \beta]$ as a circle and take care of the trace over occupation number states by including diagrams in which the fermion line winds around the circle. This is denoted by an upper integral bound $\circ\tau$. An illustration of these diagrams for $k = 3$ is shown in Fig. 1. Each end point τ_m^e is connected to a starting point τ_n^s by a dashed line representing $F(\tau_m^e - \tau_n^s)$. The collection of diagrams evaluates to

$$Z_k^F(\tau_1^s, \tau_1^e; \tau_2^s, \tau_2^e; \dots; \tau_k^s, \tau_k^e) = \det M^{-1} \delta_{\tau_1^s}^{\tau_k^e}, \quad (4)$$

$$(M^{-1})_{m,n} = F(\tau_m^e - \tau_n^s), \quad (5)$$

with $\delta_{\tau_1^s}^{\tau_k^e} = -1$ if $\tau_k^e < \tau_1^s$ (the last segment winds around the circle, as in Fig. 2 (iii)) and $+1$ otherwise. Besides the states represented by these matrices one also has to sample the ‘‘full line’’ and the ‘‘empty line’’ states, corresponding to 1 or 0 particle in the whole interval $0 \leq \tau < \beta$. Combining the $k!$ diagrams into a determinant is essential. Diagrams with an odd number of crossing F -lines have negative weight (the simplest example is the last diagram shown in Fig. 1). An algorithm which sampled individual diagrams would run into a bad sign problem, but so far we have found in all of our computations that the determinant remains positive. We discuss this issue further in the conclusion.

The following four types of Monte Carlo updates have been implemented: (i) insertion and removal of a full line, (ii) insertion and removal of a segment, (iii) insertion and removal of an anti-segment, and (iv) shift of the segment end point. While the first two updates are required for ergodicity, the last two enhance the sampling efficiency. Fig. 2 illustrates the updates (ii), (iii) and (iv).

Suppose we start with a collection of segments $s_k = (\tau_1^s, \tau_1^e; \tau_2^s, \tau_2^e; \dots; \tau_k^s, \tau_k^e)$ and want to insert a new segment \tilde{s} at a randomly chosen $\tilde{\tau}^s$. If $\tilde{\tau}^s$ happens to lie on a segment of s_k , the move to the new configuration $s_{k+1} = s_k + \tilde{s}$ is rejected, otherwise it has to satisfy the

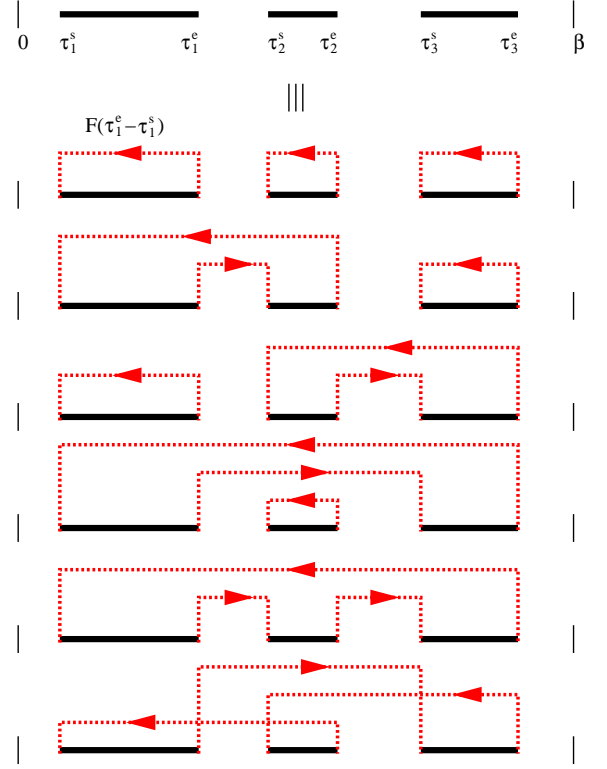


FIG. 1: Illustration of $Z_3^F(\tau_1^s, \tau_1^e; \tau_2^s, \tau_2^e; \tau_3^s, \tau_3^e)$ in terms of diagrams. A full line corresponds to an occupied fermion state. Each end point τ_m^e of a segment is connected to a starting point τ_n^s by a dashed line representing $F(\tau_m^e - \tau_n^s)$. Diagrams with an odd number of crossing dashed lines have negative weight.

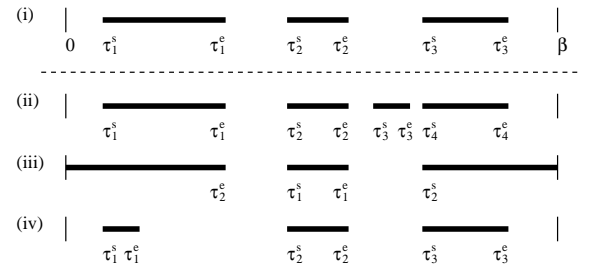


FIG. 2: Illustration of the different Monte Carlo updates: (i) original configuration, (ii) insertion of a segment at the new τ_3^s , (iii) removal of the anti-segment between τ_3^s and τ_1^s , (iv) shift of the end point τ_1^e .

detailed balance condition

$$\frac{p_{\text{ins}}^{\text{prop}}(\tilde{s})p_{\text{ins}}^{\text{acc}}(\tilde{s})}{p_{\text{rem}}^{\text{prop}}(\tilde{s})p_{\text{rem}}^{\text{acc}}(\tilde{s})} = \frac{Z_{k+1}^F(s_{k+1})}{Z_k^F(s_k)} e^{\tilde{\mu}} d\tilde{\tau}^s d\tilde{\tau}^e, \quad (6)$$

where \tilde{l} is the length of the new segment from $\tilde{\tau}^s$ to $\tilde{\tau}^e$ and p^{prop} and p^{acc} are the probabilities to propose and accept a move, respectively. If the length of the new segment is chosen randomly in the interval $[0, l_{\text{max}}]$, with l_{max} determined by $\tilde{\tau}^s$ and the collection s_k of existing segments, and we propose to remove this new segment

in the new configuration s_{k+1} with probability $1/(k+1)$, then Eq. (6) becomes

$$\frac{p_{\text{ins}}^{\text{acc}}(s_{\text{new}})}{p_{\text{rem}}^{\text{acc}}(s_{\text{new}})} = \frac{Z_{k+1}^F(s_{k+1})}{Z_k^F(s_k)} \frac{\beta l_{\text{max}}}{k+1} e^{\tilde{l}\mu}. \quad (7)$$

The result for anti-segments is similar and for shift updates from a configuration s to a configuration \tilde{s} (changing the length of some segment from l to a randomly chosen $\tilde{l} \in [0, l_{\text{max}}]$) one obtains

$$\frac{p^{\text{acc}}(s \rightarrow \tilde{s})}{p^{\text{acc}}(\tilde{s} \rightarrow s)} = \frac{Z_k^F(\tilde{s})}{Z_k^F(s)} e^{(\tilde{l}-l)\mu}. \quad (8)$$

Variants of these updates may be more suitable in certain regions of parameter space. For example, if $\mu \gg U$, one should propose the lengths of the segments according to a probability distribution $\propto \exp(-l\mu)$.

Because the ratios of determinant in Eqs. (7) and (8) can easily be computed if one knows the matrix M (the inverse of Eq. (5)), we store and manipulate M . The efficient calculation of the determinant ratios and the new enlarged (reduced) matrices in a time $O(k^2)$ is analogous to the procedure detailed in Ref. [13]. Knowing M is also essential for measuring the Green function, since

$$G(\tau) = \left\langle \frac{1}{\beta} \sum_{i=1}^k \sum_{j=1}^k M_{j,i} \Delta(\tau, \tau_i^e - \tau_j^s) \right\rangle, \quad (9)$$

$$\Delta(\tau, \tau') = \begin{cases} \delta(\tau - \tau') & \tau' > 0 \\ -\delta(\tau - \tau' - \beta) & \tau' < 0 \end{cases}. \quad (10)$$

The end points $G(0)$ and $G(\beta)$ can be measured accurately from the average total length of the segments.

For the Hubbard model with on-site interaction U , all that changes is that we now have to deal with two collections of segments, one for spin up and one for spin down, and that the probabilities for inserting/removing or shifting an (anti-)segment now also depends on the overlap between segments of opposite spin. In Eqs. (7) and (8) one has to add a factor $\exp(-\delta l_{\text{overlap}} U)$ on the right hand side, where $\delta l_{\text{overlap}}$ denotes the change in overlap between up and down segments.

We have used the new method to study the paramagnetic phase of the Hubbard model with semicircular density of states of bandwidth $4t$, for which the self-consistency condition reduces to

$$F(\tau) = t^2 G(-\tau). \quad (11)$$

We computed the local Green function and the temperature-dependent kinetic energy, which is given by $E_{\text{kin}} = 2t^2 \int_0^\beta d\tau G(\tau)G(-\tau)$. The kinetic energy results are compared to data obtained by use of the Hirsch-Fye algorithm and exact diagonalization [11, 14]. We found that low temperatures are easily accessible with the continuous-time algorithm, because it generates good

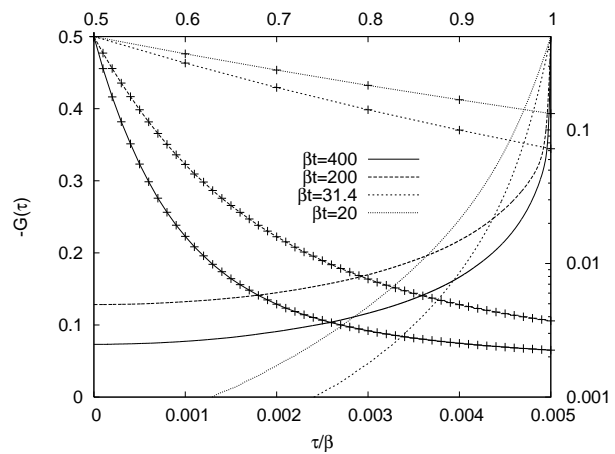


FIG. 3: Green functions for $U/t = 3.5\sqrt{2}$, $\beta t = 400, 200, 31.4$ and 20 . Lines without symbols (upper and right axes) show $G(\tau)$ on a semi-log scale over the wide time interval $[\beta/2, \beta]$. Metallic and insulating solutions differ markedly in the large τ ($\beta - \tau$) regime. Lines with symbols (lower and left axes) show the same data on a linear scale in the very narrow τ range $[0, \beta/2000]$.

statistics in the relevant regions of small and large τ (where $F(\tau)$ is strong). One can therefore nicely resolve the short-time behavior of the Green function. Simulations for temperatures down to $\beta t \approx 50$ can be run on a laptop. For calculations at $\beta t = 400$, we typically used 24 CPU hours for each iteration in order to accurately resolve the short- and long-time behavior (the latter turns out to be more time consuming).

The lines with symbols in Figure 3 show that the method accurately captures the steep drop of the Green function for $U/t = 3.5\sqrt{2}$, $\beta t = 20, 31.4, 200$ and 400 . The lower temperatures are out of reach of the Hirsch-Fye algorithm. We collected the data on a grid of 10^4 points for $\beta t = 200, 400$ and 10^3 points for $\beta t = 20, 31.4$. Despite the almost perfect resolution, the typical size k of the matrices M , which are generated during the simulation, remains reasonable even at low temperatures. Figure 4 shows the probability distribution $p(k)$ for $\beta t = 100$ and different values of the interaction strength. While the peak value of the distribution is proportional to β , it shifts to *lower* order as the interaction strength is increased, in contrast to Hirsch-Fye or the method of Ref. [13]. The linear size of the matrix is a factor of 20-100 smaller than in a Hirsch-Fye calculation with sufficient resolution, where it scales approximately as $5U\beta$. Roughly speaking, this implies that the computational effort is reduced by a factor of 20^3 - 100^3 .

Figure 5 shows the kinetic energy obtained from the three approaches plotted against T^2 . The continuous-time algorithm can handle the whole range from high to very low temperatures with relative ease, while the Hirsch-Fye results show systematic errors below $\beta t \approx 20$, presumably due to an insufficient resolution of the Green

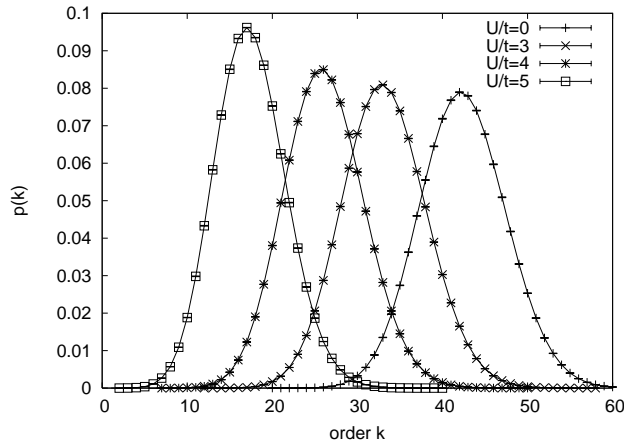


FIG. 4: Probability $p(k)$ for a configuration with k segments plotted for different interaction strengths U/t for $\beta t = 100$ and half-filling. The peak position shifts to lower values of k as U/t is increased.

function and/or long thermalization times. Our data display the metal-insulator transition clearly, agree with the Hirsch-Fye results at elevated temperatures and are roughly consistent with the exact diagonalization results at very low temperatures. The origin of the small differences remain to be determined.

In conclusion, we have developed a continuous-time impurity solver, which allows to simulate the Hubbard model at 20-100 times lower temperatures than what has been accessible with Hirsch-Fye. We are presently performing calculations away from half-filling. No sign or convergence problems have been encountered and results will be presented elsewhere. The algorithm generalizes straightforwardly to the “double-exchange” interaction with a classical core spin and to multiorbital models, with Kanamori U and U' interactions. However, a key feature of all of these models is absence of on-site exchange, so that $H_{\text{loc}} + H_{\text{mix}}$ is diagonal in the basis of orbital and spin occupation numbers. This allows us to represent expectation values of sequences of on-site operators in the convenient graphical manner outlined above, and more importantly means that in a given spin or orbital sector, the fermion operators occur in strictly alternating sequences such as $\psi_a \psi_a^\dagger \psi_a \psi_a^\dagger \dots$. We believe that this latter feature combined with the convexity of the F -function explains the absence of a sign problem in our calculations. In models with exchange (for example the quantum-spin Kondo lattice model, the multiorbital model with the full Kanamori interactions or the multisite generalizations of DMFT) a matrix formalism (to be explained elsewhere) must be used for the expectation values of local operators and, crucially, the bath fermion operators in a given sector need not occur in strictly alternating order. Whether or not this latter feature leads to a severe sign problem is the crucial open issue, and is presently under investigation.

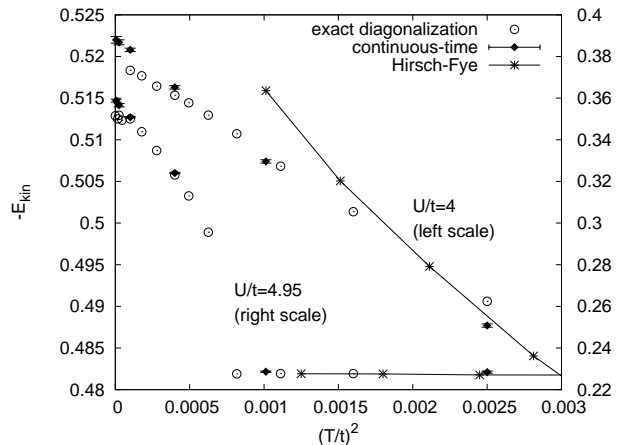


FIG. 5: Kinetic energy obtained using three different impurity solvers plotted as a function of temperature for $U/t = 4$ and $U/t = 3.5\sqrt{2} \approx 4.95$. The former value corresponds to a metallic phase, while at $U/t = 3.5\sqrt{2}$, the system undergoes a metal-insulator transition around $T/t \approx 0.026$.

PW, AC and AJM acknowledge support from NSF DMR 0431350, and LD from the Columbia-Science Po “alliance” program. We thank N. Prokof’ev, M. Rubtsov and T. Pruschke for stimulating discussions. The continuous-time calculations have been performed on the Hreidar Beowulf cluster at ETH Zürich, using the ALPS library [15].

-
- [1] E. Dagotto, *Int. J. Mod. Phys. B* **5**, 77 (1991).
 - [2] E. Y. Loh Jr. *et al.*, *Phys. Rev. B* **41**, 9301 (1990).
 - [3] S. R. White, *Phys. Rev. Lett.* **69**, 2863 (1992).
 - [4] E. Müller-Hartmann, *Z. Phys.* **B74** 507 (1989).
 - [5] M. Metzner and D. Vollhard, *Phys. Rev. Lett.* **62**, 324 (1989).
 - [6] A. Georges and G. Kotliar *Phys. Rev. B* **45**, 6479 (1992).
 - [7] A. Georges, G. Kotliar, W. Krauth and M. J. Rozenberg, *Rev. Mod. Phys.* **68**, 13 (1996).
 - [8] T. Maier, M. Jarrell, T. Pruschke, and M. H. Hettler, *Rev. Mod. Phys.* **77**, 1027 (2005).
 - [9] J. E. Hirsch and R. M. Fye, *Phys. Rev. Lett.* **56**, 2521 (1986).
 - [10] M. Caffarel and W. Krauth, *Phys. Rev. Lett.* **72**, 1545 (1994).
 - [11] A. Toschi, M. Capone, M. Ortolani, P. Calvani, S. Lupi, and C. Castellani, *Phys. Rev. Lett.* **95**, 097002 (2005).
 - [12] N. V. Prokof’ev, B. V. Svistunov and I. S. Tupitsyn, *JETP Lett.* **64**, 911 (1996).
 - [13] A. N. Rubtsov, V. V. Savkin and A. I. Lichtenstein, *Phys. Rev. B* **72**, 035122 (2005).
 - [14] M. Capone, L. de Medici, and A. Georges, *cond-mat/0512484*.
 - [15] M. Troyer *et al.*, *Lecture Notes in Computer Science* **1505**, 191 (1998); F. Alet *et al.*, *J. Phys. Soc. Jpn. Suppl.* **74**, 30 (2005); <http://alps.comp-phys.org/> .